PLANETARY SCIENCE

Protracted core formation and impact disruptions shaped the earliest outer Solar System planetesimals

Damanveer S. Grewal[1,2,3]*, Zhongtian Zhang[4], Varun Manilal[1,3], Thomas S. Kruijer[5], William F. Bottke[6], Sarah T. Stewart[3]

The distinct compositions of metallic cores from noncarbonaceous (NC) and carbonaceous (CC) iron meteorite parent bodies (IMPBs) reflect differences in accretion and differentiation histories of earliest inner and outer Solar System planetesimals. Compared to NC IMPBs, CC IMPBs have smaller, sulfur (S)–poor, highly siderophile element (HSE)–enriched cores and younger core formation ages. However, the origins of these differences remain debated. Using equilibrium partitioning models between the S-poor solid and the S-rich liquid metal, we argue that HSE enrichment in IID, IIF, IIIF, and IVB cores resulted from a multistage evolutionary sequence: (i) segregation of S-rich, HSE-depleted protocores during initial planetesimal heating; (ii) collisional disruption before S-poor metal segregation; (iii) reaccretion of mantle fragments into daughter planetesimals; and (iv) further ^{26}Al-driven heating producing HSE-enriched, S-poor cores. We suggest that iron meteorites from these CC IMPBs originate from such second-generation cores. Accounting for "missing" S-rich protocores helps reconcile several NC-CC IMPB differences and highlights the role of early collisional processing in shaping planetesimal chemical evolution.

INTRODUCTION

Magmatic iron meteorites are key to understanding the formation and evolution histories of the earliest Solar System planetesimals across space and time. They are remnants of the metallic cores of planetesimals which formed shortly after the first Solar System solids [calcium-aluminum–rich inclusions (CAIs)] and underwent core-mantle differentiation driven by the decay of ^{26}Al (*1*–*6*). Similar to chondrites and achondrites, iron meteorites exhibit an isotopic dichotomy: noncarbonaceous (NC) iron meteorite parent bodies (IMPBs) formed in the inner Solar System and carbonaceous (CC) IMPBs formed in the outer Solar System, likely beyond Jupiter's original orbit (*1*). Despite the isotopic dichotomy, the abundances of moderately (e.g., Ge and Ga) and highly (e.g., C and N) volatile elements in NC and CC IMPBs are not substantially different (*7*–*14*), implying that they accreted from compositionally similar primordial materials (*15*, *16*). However, NC and CC IMPBs have certain distinct chemical signatures that hint at potential differences in their accretion and differentiation histories. For instance, CC IMPBs are inferred to have smaller, S-poor cores that are enriched in highly siderophile elements (HSEs; Os, Re, Ir, Ru, Rh, Pt, and Pd) and may have younger core formation ages when compared to NC IMPBs (*1*, *7*, *8*, *17*–*20*). If NC and CC IMPBs formed from broadly similar materials in comparable environments (*15*, *16*, *21*), what is the cause behind these differences? Do their properties reflect fundamental differences in the formation and evolution histories of the earliest inner and outer Solar System planetesimals (*7*, *18*, *22*, *23*), or are they the result of secondary processes that overprinted common accretion histories?

Unlike other siderophile elements, the S content in the IMPB cores is inferred indirectly from fractional crystallization models (*24*–*26*), which interpret elemental correlations among siderophile and chalcophile elements (e.g., Au, Ir, and As) using extensive datasets generated by Wasson and colleagues at the University of California, Los Angeles over several decades. These models predict that NC cores were systematically S-rich (3 to 15 wt % S; mean: 9.8 wt % S) compared to CC cores (0 to 8 wt % S; mean: 3.5 wt % S) (table S1) (*7*, *8*, *17*, *24*, *26*). This discrepancy is intriguing, as CC IMPBs, which formed in the outer, colder regions of the solar protoplanetary disk, would be expected to have accreted materials enriched in moderately volatile elements (MVEs) like S (*27*). Unexpectedly, the IID and IVB cores from the CC reservoir are predicted to be almost S-free (*7*, *21*). Note that for the IVB core, similar depletions are observed for other MVEs, such as Ga and Ge, whereas the IID core does not exhibit anomalous MVE depletion, except for S (*7*, *26*, *28*). Understanding the difference between S contents in NC and CC cores is also critical because both the mechanism and timing of planetesimal core formation are directly tied to the S content in the core (*1*, *2*). Laboratory experiments show that the first melting in the Fe-FeS system occurs at the eutectic (~980°C at 1 bar), producing S-rich metallic liquids (*29*–*33*). Combined with siderophile element depletion patterns observed in primitive achondrites, this suggests that the percolation of S-rich metallic liquids initiated early episodes of protocore formation in largely unmolten silicate mantles (*34*–*37*). However, while percolative metal-sulfide migration is well documented in some primitive achondrites, direct geochemical evidence for low-temperature (relative to the melting of pure iron), percolative core formation in IMPBs is lacking. An inverse correlation between the S content in the parent cores of NC IMPBs and their ε^{182}W values suggests that these bodies could have experienced distinct early and late episodes of S-rich and S-poor metallic liquid segregation, respectively, with the contribution of each episode dictated by the final S content in their parent cores (fig. S1) (*1*, *2*, *18*). Therefore, the younger core formation ages of CC IMPBs could potentially be linked to the lower S content in their parent cores, which led to a smaller contribution from the early-segregated S-rich component to

[1]Department of Earth and Planetary Sciences, Yale University, New Haven, CT 06511, USA. [2]School of Molecular Sciences, Arizona State University, Tempe, AZ 85281, USA. [3]School of Earth and Space Exploration, Arizona State University, Tempe, AZ 85281, USA. [4]Earth and Planets Laboratory, Carnegie Institution for Science, Washington, DC 20015, USA. [5]Lawrence Livermore National Laboratory, Livermore, CA 94550, USA. [6]Solar System Science & Exploration Division, Southwest Research Institute, Boulder, CO 80302, USA.
*Corresponding author. Email: damanveer.grewal@yale.edu

their $\varepsilon^{182}W$ values (*2*). However, unlike NC IMPBs, the S content in the parent cores of CC IMPBs and their $\varepsilon^{182}W$ values do not show any correlation (fig. S1) (*18*). For instance, the S-free IID and IVB cores display broadly similar $\varepsilon^{182}W$ values to S-bearing (2 to 6 wt % S) IIC, IIF, and IIIF cores, while the South Byron Trio (SBT) core containing 8 wt % S exhibits a substantially lower $\varepsilon^{182}W$ value. The reason for the absence of a correlation between $\varepsilon^{182}W$ values and S content in CC cores is currently unknown.

In addition, CC cores are notably enriched in HSEs compared to their NC counterparts (*7*, *8*, *17*). This enrichment has been attributed to the differences in their inferred core mass fractions, with NC IMPBs consistently having higher core mass fractions (0.14 to 0.24; mean: 0.19) compared to CC IMPBs (0.03 to 0.17; mean: 0.08) (table S1; see Materials and Methods for details) (*17*, *19*, *20*). Notably, the S-free IID and IVB cores exhibit anomalously low core mass fractions (0.05 and 0.03, respectively). Moreover, while NC cores display near-chondritic HSE/Ni_{CI} ratios (HSE abundances normalized to Ni and CI chondrites), four of six CC cores, including IID, IIF, IIIF, and IVB, have superchondritic HSE/Ni_{CI} ratios (*7*, *8*, *23*). The IID and IVB cores not only exhibit the highest HSE/Ni_{CI} ratios but also show HSE fractionation trends that correlate with volatility, with HSE/Ni_{CI} ratios decreasing progressively from Os to Pd (*7*, *8*, *28*). Similar patterns are also observed in the IIIF core and, to a lesser extent, in the IIF core (*7*, *8*). In the IVB core, this sloped pattern has been linked to the accretion of CAIs—high-temperature condensates that exhibit similar HSE fractionation trends with volatility (*23*, *28*). Recent studies linking Os/Ni_{CI} or Ir/Ni_{CI} ratios with CAI abundance in CC chondrites suggest that the superchondritic HSE/Ni_{CI} ratios in the IID, IIF, IIIF, and IVB cores were tied to the presence of ~9 to 26 vol % CAIs in the primordial materials accreted by their parent bodies (*7*, *8*). The presence of CAI-enriched materials in CC IMPBs (except for IIC and SBT) was further used to infer the structure and evolution of the solar protoplanetary disk. Although spectroscopic observations suggest that some asteroids may contain up to 30 vol % CAIs (*38*), there is no direct evidence of such CAI-enriched materials in the meteorite record.

The Mo isotopic composition of CAIs provides an important constraint on the extent to which the CAI-rich material was accreted by CC IMPBs. Like HSEs, the Mo/Ni_{CI} ratios in the IID, IIF, IIIF, and IVB cores are superchondritic (*7*, *28*). The elevated abundances of Mo in CAIs coincide with their enrichment in *r*-process Mo isotopes compared to bulk CC meteorites (*39*) [reported as $\Delta^{95}Mo$, which isolates variations of *r*-process Mo from *s*-process Mo and is denoted as $\Delta^{95}Mo = (\varepsilon^{95}Mo - 0.596 \times \varepsilon^{94}Mo) \times 100$ (*40*)]. For instance, Mo-enriched CAIs exhibit high $\Delta^{95}Mo$ values (commonly >100), contrasting with the mean $\Delta^{95}Mo$ of ~25 for bulk CC meteorites (*39*). If the IVB core had accreted ~26 vol % CAIs, as suggested by refs. (*7*, *8*), its Mo isotopic signature should reflect a strong *r*-process excess. However, IVB irons show $\Delta^{95}Mo$ values indistinguishable from other CC meteorites (*1*). Notably, the multi-isotope mixing models of ref. (*41*) predict relatively modest fractions of CAIs (~3.5 to 5.5 wt %) in CC IMPBs. While we acknowledge the debate on Mo isotope measurements (*40*, *42*), the lack of a $\Delta^{95}Mo$ anomaly in IVB irons, despite their elevated Mo/Ni_{CI} ratio, casts doubt on a dominant CAI source for CC IMPBs.

The superchondritic HSE/Ni_{CI} ratios observed in the IID, IIF, IIIF, and IVB cores are also present in primitive achondrites such as ureilites (*34*–*37*), which are mantle restites formed after the extraction of S-rich metallic liquids and low-degree silicate melts (*43*, *44*). These superchondritic HSE/Ni_{CI} ratios have been attributed to equilibrium partitioning between S-poor solid metal restites and S-rich metallic liquids, followed by the segregation of S-rich liquids to form protocores (see Materials and Methods for details). However, a key difference exists between the HSE/Ni_{CI} patterns in ureilites and those in the IID, IIF, IIIF, and IVB cores. Unlike these CC cores, where HSE/Ni_{CI} ratios show strong fractionation correlated with their volatility, primitive achondrites, such as ureilites, exhibit limited fractionation among HSE/Ni_{CI} ratios, except for the more volatile Pd.

In this study, we model the equilibrium partitioning of HSEs, Ni, and Co between the S-poor solid metal and the S-bearing metallic liquid to demonstrate that the superchondritic HSE/Ni_{CI} ratios and their volatility-related fractionation in the IID, IIF, IIIF, and IVB cores can be explained by planetesimal core formation processes without the need to invoke the accretion of exotic CAI-enriched materials. Given that core formation in a planetesimal is tied to the S content in its core, which in turn is linked to its core formation mechanism and age, our findings reconcile several apparent discrepancies in the chemical signatures between NC and CC IMPBs. These results offer previously unrecognized insights into the differentiation histories of the earliest outer Solar System planetesimals and their interplay with the dynamics of planetesimal collisions in the early Solar System.

Numerical Models

The approach used for explaining the HSE abundances in primitive achondrites, which involves analyzing correlations between HSE ratios (e.g., Pd/Os_{CI} and Pt/Os_{CI}) across multiple samples (*34*–*36*), cannot be applied here because of the absence of comparable data for IMPB cores, where constraints exist only for the bulk core compositions. Instead, we aim to determine whether the bulk abundance patterns of HSEs, Ni, and Co in the IID, IIF, IIIF, and IVB cores can be explained by equilibrium partitioning between the S-free solid and the S-bearing liquid metal. Unlike previous studies on primitive achondrites that focused solely on HSE fractionation (*34*–*36*), we include Ni and Co—refractory elements with similar volatility to Pd—in our models (*45*). Ni and Co are valuable constraints because, unlike HSEs, these elements are not concentrated in the refractory metal component of CAIs (*45*). As a result, they offer a stringent test for the models that propose the accretion of CAI-rich materials to explain the superchondritic HSE/Ni_{CI} ratios observed in the IID, IIF, IIIF, and IVB cores. Given that HSEs, Ni, and Co have high metal/silicate partition coefficients (>10^2 to 10^4) at the low pressures relevant for planetesimal differentiation (*15*, *16*, *28*), we only need to consider their equilibrium partitioning between the S-free solid and the S-bearing liquid metal despite the partitioning taking place in the presence of silicates (*34*, *36*).

To assess the applicability of our approach, we first modeled the equilibrium partitioning of HSEs, Ni, and Co during batch melting of S-free solid metal with a S-bearing metallic liquid using parametrized $D_i^{S/L}$ (partition coefficient of an element between solid and liquid metal) equations from ref. (*46*) to predict the abundance patterns of these elements in the well-studied ureilites (see Materials and Methods for details). Using the same methodology, we

investigated whether the IID, IIF, IIIF, and IVB cores represent solid metal restites left after the extraction of S-bearing liquids during an earlier stage of low-temperature, percolative core formation. We used the Bayesian Markov Chain Monte Carlo (MCMC) approach to determine the common S content in the liquid metal and the mass ratio of solid to liquid metal (m_S/m_L) that best replicates the observed abundances of HSEs, Ni, and Co in the restite component (see Materials and Methods for details).

RESULTS

The solid metal restite component of our single-stage batch model matches well with the abundances of HSEs, Ni, and Co in ureilites (Fig. 1A). Our model predicts that the bulk composition of ureilites, derived from chondrite-like precursors, can be best explained by the extraction of ~85% of the initial metal as a liquid containing ~27 wt % S (table S2). This result is consistent with predictions from ref. (*34*), which are based on correlations between Pd/Os_{CI} and Pt/Os_{CI} ratios

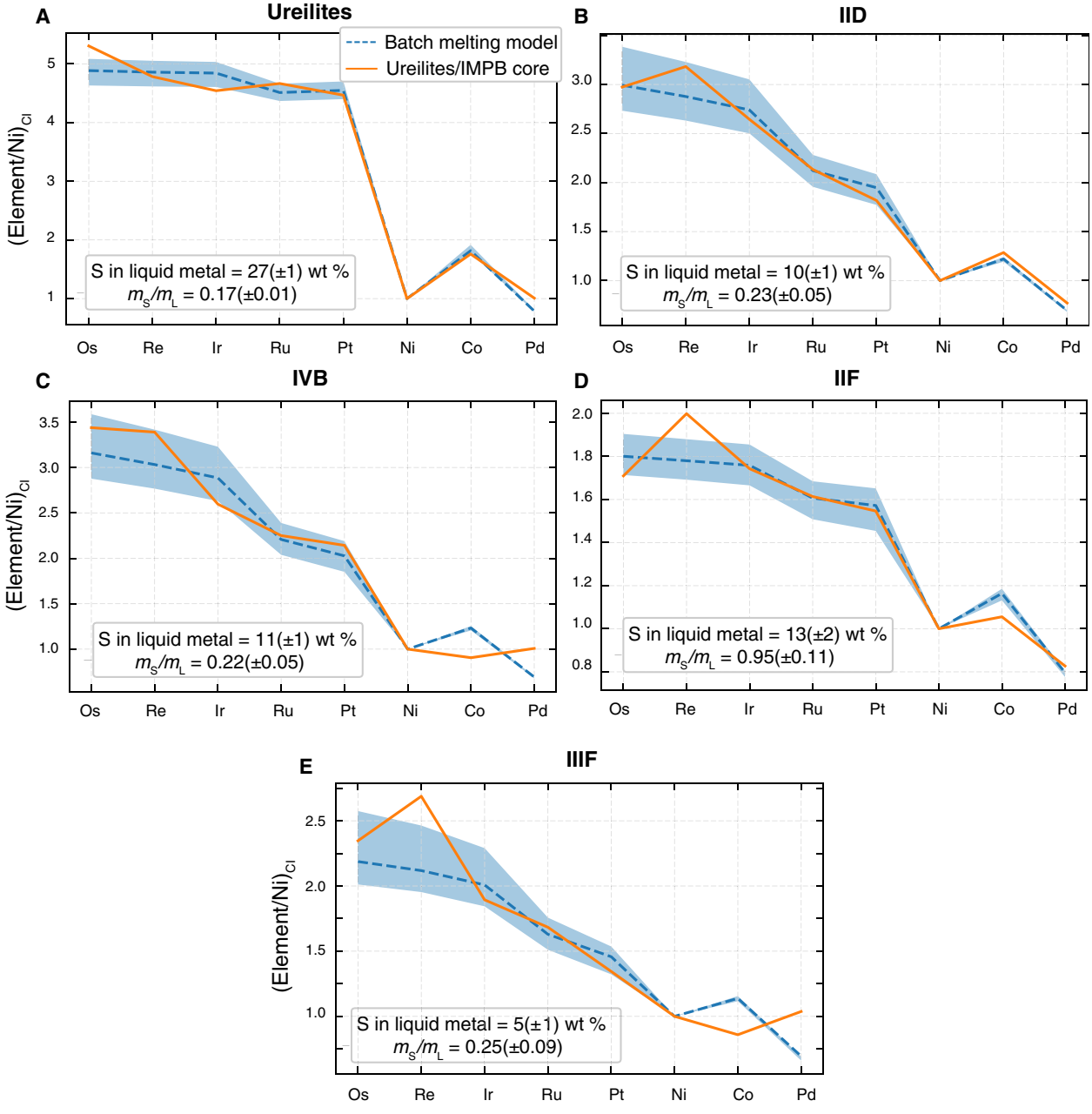

Fig. 1. Comparisons of the Ni- and CI chondrite–normalized elemental abundances of ureilites and IID, IVB, IIF, and IIIF IMPB cores (solid orange lines) with the results of batch melting models between the S-free solid restite and the S-bearing liquid (dashed blue lines). Our batch melting models for varying S content in the liquid metal and mass ratios of solid and liquid metal (m_S/m_L) can broadly reproduce the abundance patterns of HSEs, Ni, and Co in ureilites (**A**) and CC IMPB cores (**B** to **E**). The dashed blue lines represent model outputs generated using the mean parameter values from the MCMC posterior distributions, while the blue bands indicate the 1σ range of model predictions reflecting uncertainties in the S content and m_S/m_L. The mean values and 1σ uncertainties shown in each panel were derived from these posterior distributions obtained using a Bayesian MCMC approach.

across multiple samples and suggest the extraction of up to ~80% of the initial metal as a liquid containing ~20 to 25 wt % S. Extending our models to CC IMPBs, we demonstrate that the HSE, Ni, and Co abundances in the IID and IVB cores can be attributed to a metal restite component formed after the extraction of ~81 and ~82% of the initial metal as a liquid containing ~10 and ~11 wt % S, respectively (Fig. 1, B and C, and table S2). The IIF core is best fit by the extraction of ~51% of the initial metal as a liquid with ~13 wt % S, while the IIIF core composition can be explained by the extraction of ~80% of the initial metal as a liquid with ~5 wt % S (Fig. 1, D and E, and table S2). Analogous to ureilites, our single-stage batch model is able to almost perfectly reproduce the abundance patterns of almost all HSEs in the IID core (Fig. 1B), whereas for IIF, IIIF and IVB cores, even though our model can explain the overall fractionation trends among HSEs, the abundances of some elements are either over- or underpredicted. For instance, our models underpredict Re/Ni_{CI} in the IIF and IIIF cores and Pd/Ni_{CI} ratios in the IIIF and IVB cores but overpredict the Co/Ni_{CI} ratios in all three (Fig. 1, C to E). These discrepancies may arise either from limitations in the fractional crystallization models used to predict the elemental abundances in the IMPB cores or from additional complexities in the planetesimal core formation process.

DISCUSSION

The variations in both the S content and mass fraction of the extracted liquid are controlled by the interplay between their HSE, Ni, and Co abundance patterns and the solid/liquid metal partition coefficients of these elements as a function of the S content in the metallic liquids. While the amount of extracted liquid required to account for the compositions of IID and IVB cores is comparable to that for ureilites, the HSE, Ni, and Co abundances in these cores require the extracted liquid to contain less than half the S needed for ureilites (Fig. 1). This is mainly due to the strong relative fractionation of HSE/Ni_{CI} ratios in the IID and IVB metals compared to ureilites, which have broadly unfractionated HSE/Ni_{CI} ratios, except for Pd. Given that all HSEs, except Pd, have very high solid/liquid metal partition coefficients when the equilibrating liquid is very S-rich (fig. S2), relative fractionation of HSE/Ni_{CI} ratios would be limited, as observed in ureilites. Substantial fractionation among HSEs can only occur when these elements become less compatible in the solid metal, meaning that the equilibrating liquid metal must be relatively S-poor. Note that the relatively S-poor composition of the extracted liquids in IID, IIF, IIIF, and IVB cores, compared to ureilites, is likely a result of higher temperatures at which the S-bearing liquid metal equilibrated with the solid restite on average. This is because at higher temperatures, the composition of the liquid metal becomes progressively depleted in S according to the Fe-S phase diagram (*47*).

It is important to highlight that the IID core is the only CC core with a distinctly superchondritic Co/Ni_{CI} ratio (1.32), whereas the Co/Ni_{CI} ratios of all other CC cores lie in the chondritic range (Fig. 1B). The Co/Ni_{CI} ratios of the IID core are too high to be directly derived from any known chondrite group, as Co/Ni_{CI} ratios in CC chondrites typically range from 0.95 to 1.00 (*34*, *36*). Given that both Ni and Co near-quantitatively partition into IMPB cores, as attested by the chondrite-like Co/Ni_{CI} ratios in other CC cores (*15*), the superchondritic Co/Ni_{CI} ratio in the IID core cannot be explained by metal-silicate differentiation processes. However, Co is more compatible than Ni in the solid metal when equilibrating with S-rich liquids, and its compatibility increases at a higher rate with increasing S content in the liquid metal (fig. S2). The high fractionation of Co/Ni_{CI} ratio in ureilites (1.80) (Fig. 1A), because of the higher S content in the extracted metallic liquid (~27 wt % S), supports the applicability of this process. Similar superchondritic Co/Ni_{CI} ratios are present in all other primitive achondrites such as acapulcoites, lodranites, brachinites, and winonaites (*34*–*37*). Given that the origin of siderophile element abundance pattern in primitive achondrites is well established to result from the extraction of S-rich liquids, the superchondritic Co/Ni_{CI} ratio in the IID core strongly suggests that the fractionation between its Co and Ni contents is linked to its origin as a solid metal restite component that equilibrated with S-rich metallic liquids (*26*). The IIIF and IVB cores, and to a lesser extent, the IIF core, do not display superchondritic Co/Ni_{CI} ratios despite their HSE/Ni_{CI} ratios being explained by solid-liquid metal partitioning and their broadly similar HSE fractionation trends as the IID core (Fig. 1, C to E). Whether this discrepancy arises from the limited resolution of fractionation crystallization models [e.g., the inability of these models to explain Co variations in IIIF irons (*48*)] or from additional fractionation processes [e.g., Co/Ni fractionation during catastrophic volatile loss in the extremely volatile-depleted IVB and IIIF cores, similar to what is observed in the metal component of CB chondrites (*49*)] remains unclear and requires further investigation.

In conclusion, the HSE, Ni, and Co abundance patterns in the IID, IIF, IIIF, and IVB cores can be explained by their origin from a solid metal restite component that was left behind after the extraction of S-rich metallic liquids during an earlier stage of low-temperature protocore formation. Given that the IID and IVB cores are inferred to be nearly S-free (*7*, *24*, *26*, *50*), their entire S inventories must have undergone near-total extraction into S-rich protocores that are now lost. In contrast, for the S-bearing IIF (5 wt % S) and IIIF (2 wt % S) cores, not all of the S inventories were removed into the early-formed S-rich protocores. Evidence for the latter is also present in primitive achondrites, which retain varying amounts of sulfides in the restite component (*43*, *44*). Although core formation in planetesimals was likely a protracted process involving multiple S-rich liquid extraction events (*30*, *35*, *37*), our simple single-stage batch model, which is an approximate average of all these extraction events, successfully reproduces their overall HSE, Ni, and Co abundance patterns. The early-segregated S-rich liquid protocore component did not contribute to the core compositions inherited from the late-segregating S-poor restites, which were eventually sampled by iron meteorites from the IID, IIF, IIIF, and IVB groups. We demonstrate that volatility-related HSE fractionation trends in the IID, IIF, IIIF, and IVB cores can be attributed to the geochemical legacy of protracted core formation, as the partitioning of these elements between solid and liquid metal, depending on the S content in the latter, unexpectedly correlates with their volatility. Consequently, the superchondritic HSE/Ni_{CI} ratios and their volatility-related fractionation in the CC cores can simply be explained by the intricacies of planetesimal core formation without needing to invoke the accretion of exotic CAI-enriched materials by their parent bodies, as suggested by refs. (*7*, *8*, *23*).

Role of early planetesimal collisions in shaping the core compositions of CC irons

The IID, IIF, IIIF, and IVB irons sample cores formed from the restite component, with minimal contribution from the early-extracted

S-rich metallic liquid. This suggests that the S-rich liquid segregated to form protocores in the progenitor bodies before the melting and segregation of S-poor restites. The S-depleted CC IMPBs originated from S-poor restites hosted in the mantles of the progenitors. This scenario suggests that partially molten planetesimals experienced early disruptions within a narrow time frame—after S-rich protocore segregation but before S-poor restite melting—followed by reaccretion of impact fragments into daughter bodies. The collisions may have been energetic enough to generate daughter bodies, largely excluding fragments from the S-rich protocores in those sampled by CC IMPBs (Fig. 2A). Alternatively, hit-and-run collisions with nearby protoplanets may have stripped away the progenitor's outer layers (Fig. 2B) (*51*–*54*), forming daughter bodies dominated by mantle material, while the S-rich core and some mantle remained with the remnant. Determining whether daughter bodies are more likely to form from high-energy impacts or hit-and-run collisions involving protoplanets requires further investigation. However, dynamical models and meteorite evidence suggest that hit-and-run events may be more likely (*52*, *54*, *55*).

Ureilites provide meteoritic evidence of the early disruption of a partially molten parent planetesimal, with the meteorites originating from the subsequent reassembly of daughter bodies from the collisional fragments (*56*–*59*). All ureilite materials in our meteorite collection are thought to originate from a single ureilite parent body (UPB), which experienced low-degree melting, leading to the segregation of a S-rich protocore and the formation of a trachyandesitic crust (*37*, *43*, *56*). On the basis of the thermal history of ureilites, marked by rapid cooling from high temperatures of ~1050° to 1100°C, the breakup of the UPB occurred while it was partially molten (*57*–*60*).

Although ureilites originate from the NC reservoir (*61*), high-energy impacts or hit-and-run collisions in the CC reservoir could explain the geochemical signatures of the IID, IIF, IIIF, and IVB irons, given the high frequency of collisions in the early Solar System. The progenitor parent bodies of these CC IMPBs must have experienced these collisions after the segregation of the S-rich protocores and before the melting and segregation of S-poor restites. Therefore, the IID, IIF, IIIF, and IVB IMPBs likely represent daughter bodies that reaccreted from the collisional fragments. However, a key distinction between the impact disruption of their progenitor parent bodies and that of the UPB is the timing. The reaccreted daughter bodies for ureilites remained as rubble pile bodies, experiencing little igneous processing after their reaccretion (*56*, *58*). Therefore, the disruption of UPB, and the subsequent reaccretion of daughter bodies, could have taken place as late as ~5 million years (Ma) after CAIs when ^{26}Al was extinct (*56*). However, a late disruption and reaccretion pose a challenge for the progenitor parent bodies of the IID, IIF, IIIF, and IVB IMPBs, as their daughter bodies

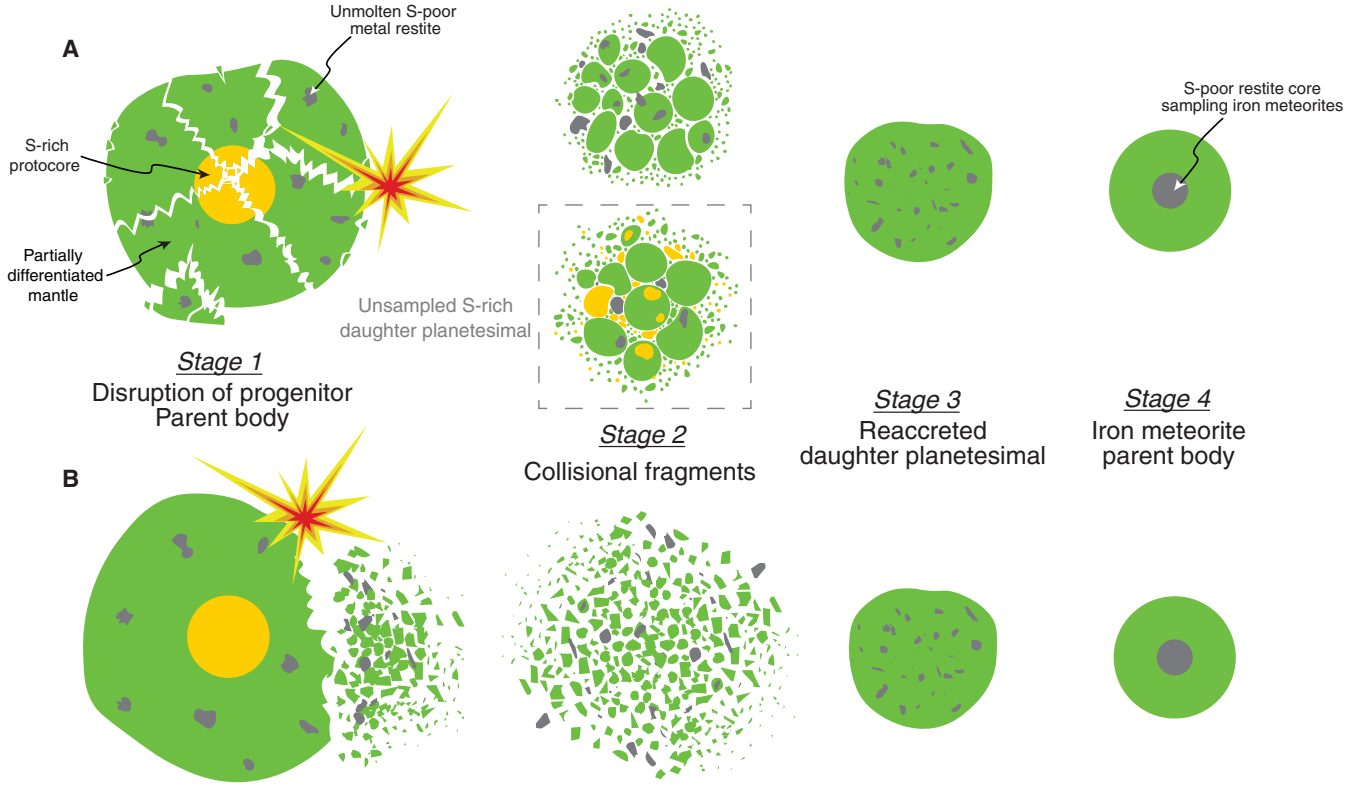

Fig. 2. Illustration of the proposed formation mechanisms for the formation of IID, IIF, IIIF, and IVB daughter IMPBs following the collisional disruption of their progenitor parent bodies. (**A**) and (**B**) depict disruptions via high-energy impacts and hit-and-run collisions, respectively. Stage 1: A partially differentiated planetesimal heated by ^{26}Al decay, featuring an S-rich protocore and S-poor solid metal stranded in its mantle, undergoes disruption. Stage 2: Collisional fragments begin to reaccrete into daughter planetesimals. In the high-energy impact scenario, daughter planetesimals formed from fragments containing S-rich protocore components (dashed square) are not sampled in the meteorite record. Stage 3: The daughter planetesimals reaccreted from the mantle fragments heat up because of the radiogenic decay of residual ^{26}Al. Stage 4: The daughter planetesimals (IID, IIF, IIIF, and IVB IMPBs) differentiate, forming S-poor cores that are later sampled as iron meteorites.

need to undergo another stage of core formation involving the S-poor restite, which is eventually sampled in the iron meteorite record. To achieve this, the daughter planetesimals would need to reach the liquidus temperature of the S-poor restite, estimated at 1500° to 1530°C (*62*)—a temperature greater than that experienced by the progenitors before their disruption. Therefore, the disruption must have occurred while the decay of ^{26}Al was still active, i.e., within ~3 Ma after CAIs.

The core formation ages of the IID, IIF, IIIF, and IVB irons (~3 to -3.6 Ma after CAIs) (*18*) set a strict upper limit on the timing of the disruption events, as core formation in the daughter bodies must occur after these disruptions. The exact timing of disruptions depends on several factors, including the initial temperature of the reaccreted daughter rubble pile. For example, if the daughter planetesimal reaccreted at a cold temperature (0°C) and needed a temperature rise of ~1500°C to initiate core formation, the disruption events should have occurred within ~1 Ma after CAIs (fig. S3; see Materials and Methods for details). However, if only a ~250° to 500°C increase was required, the disruption events could have occurred as late as ~2 to 2.5 Ma after CAIs. This indicates that the progenitor parent bodies of IID, IIF, IIIF, and IVB IMPBs were disrupted very early in the Solar System history, likely within ~1 to 2.5 Ma after CAIs.

Implications for the chemical signatures of the earliest outer Solar System planetesimals

The compositions of CC irons have been previously used to infer key physical and chemical properties of the earliest Solar System planetesimals, including core mass fractions, bulk oxidation states, core formation ages, and S content in parent cores. Our results indicate that the IID, IIF, IIIF, and IVB irons, which sample only the S-poor restite component of the progenitor parent bodies, likely originated from the cores of daughter bodies that reaccreted from mantle fragments of partially differentiated progenitors. Given that these CC irons represent only partial samples of the bulk metal of their progenitors, relying solely on their compositions to reconstruct the primordial characteristics of the earliest outer Solar System planetesimals may lead to erroneous conclusions. Therefore, it is crucial to retrace the chemical compositions of the bulk metal of the progenitor parent bodies of the IID, IIF, IIIF, and IVB irons to properly contextualize their characteristics and achieve a more accurate understanding of the earliest outer Solar System planetesimals.

Core mass fractions and bulk oxidation states of IMPBs

The extent of HSE enrichment in IMPB cores relative to chondrites has been used to determine the core mass fractions of the earliest Solar System planetesimals (*17*). These estimates rely on the assumption that all HSEs accreted by IMPBs were extracted into cores during a single-stage differentiation event and that these cores are sampled by iron meteorites, an assumption we now argue may not hold universally. Given that CC cores are more enriched in HSEs than NC cores, the earliest outer Solar System planetesimals are predicted to have lower core mass fractions, indicating that they were more oxidized than their NC counterparts (*17*, *18*). Specifically, the IID and IVB IMPBs are found to have particularly low core mass fractions (0.05 and 0.03, respectively) (Fig. 3A and table S1). The core mass fraction estimates have been further combined with the Fe/Ni ratios of the cores to quantify the amount of oxidized Fe in IMPB mantles, providing insights into their bulk oxidation states (*15*). However, the superchondritic HSE/Ni$_{CI}$ ratios call into

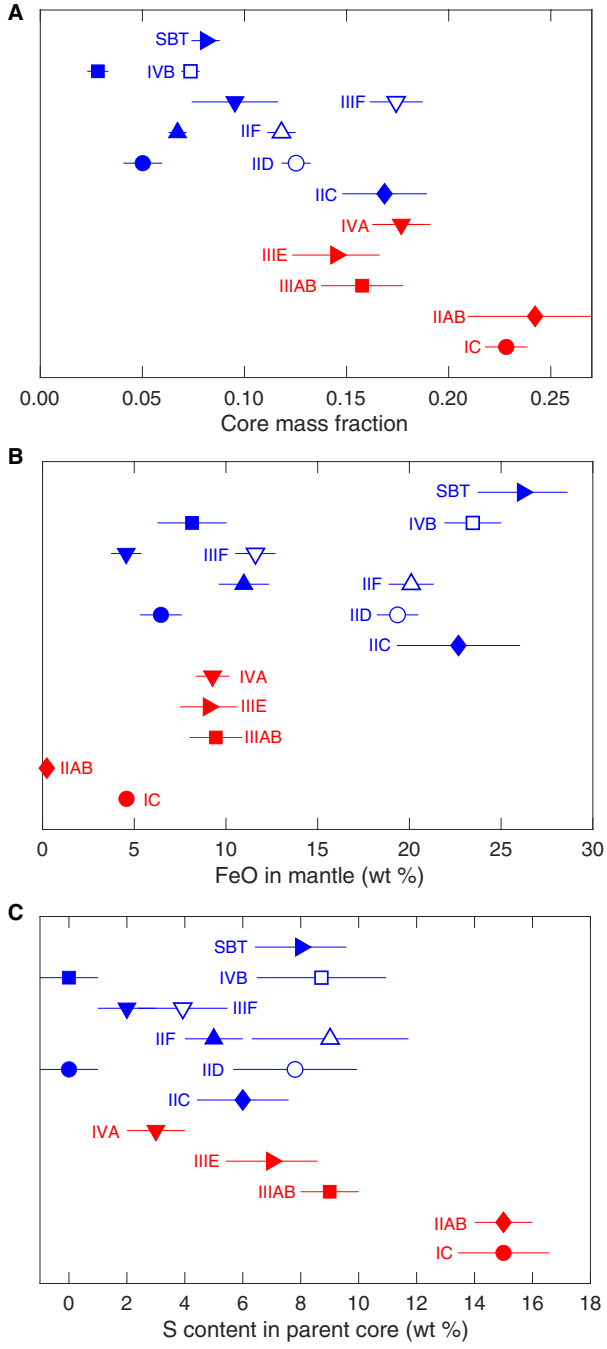

Fig. 3. Comparison of the reconstructed core mass fractions, FeO in mantles, and S content in cores of the progenitor parent bodies of IID, IIF, IIIF, and IVB (open symbols) with values directly determined from iron meteorite data (solid symbols) for NC and CC IMPBs (red and blue colors, respectively). The reconstructed values for all three parameters are significantly higher than previously estimated for IID, IIF, IIIF, and IVB IMPBs. (**A**) The reconstructed core mass fraction for IVB overlaps with SBT and those of IID and IIF overlap with IIC, whereas the reconstructed core mass fractions for IIIF are higher than all CC IMPBs and overlap NC IMPBs. (**B**) The reconstructed FeO content of the mantles suggests that the earliest CC planetesimals (except IIIF) had consistently higher FeO content in their mantles compared to NC planetesimals. (**C**) The reconstructed S content in the progenitor parent cores of IID, IIF, IIIF, and IVB overlaps with that of other CC groups (IIC and SBT) and several NC groups (IIIAB, IIIE, and IVA). Error bars represent 1σ uncertainties propagated from individual terms.

question the approach of ref. (*12*) to estimate the core mass fractions of CC IMPBs on the basis of HSEs alone. For instance, on the basis of Ni, a siderophile refractory element that, like HSEs, partitions near quantitatively into the cores during CC IMPB differentiation (*16*, *33*), the core mass fractions of IID and IVB IMPBs would be nearly twice as high (0.09 and 0.06, respectively).

Our findings suggest that using HSE abundances to constrain core mass fractions may yield erroneous conclusions for IID, IIF, IIIF, and IVB irons, as these samples represent only the late-segregated, S-poor restite component of the daughter bodies rather than the entire parent cores. Given that our models estimate both the mass fraction and chemical composition of the "missing" component, a mass balance approach can be used to calculate the bulk HSE, Ni, and Co abundances in the parent cores of the progenitor parent bodies of CC IMPBs, assuming that no early disruptions occurred before complete core-mantle segregation. By factoring in the "missing" component, the recalculated core mass fractions for the progenitor parent bodies of IID, IIF, IIIF, and IVB irons are 0.13, 0.12, 0.17, and 0.07, respectively (Fig. 3A and table S1). Although the estimated core mass fractions of the progenitor CC parent bodies remain somewhat lower than those of NC IMPBs, they are still considerably higher than estimates based solely on the restite components sampled by iron meteorites. This approach resolves the previously puzzling anomaly of the unusually low core mass fraction in the IVB IMPB. For instance, our results reveal that the core mass fraction of the progenitor parent body of IVB (0.07) was almost identical to that of the SBT IMPB (0.08), with both cores exhibiting similarly low Fe/Ni ratios (4.0 to 4.5) compared to the other CC cores (7.8 to 11.0).

Our findings also call for revisions to the estimated amount of oxidized iron in the mantles of IMPBs, as these values directly correlate with core mass fractions of IMPBs [$C_{Fe}^{mantle} = [\left(\frac{Fe}{Ni\ or\ Co}\right)^{bulk} \times C_{Ni\ or\ Co}^{core} - C_{Fe}^{core}] \times r$, where r is the core/mantle mass ratio; for details, see ref. (*15*)]. Given that our revised core mass fractions are higher, the mantles of the progenitor parent bodies of IID, IIF, IIIF, and IVB irons contained significantly more oxidized Fe than previously estimated (Fig. 3B and table S1). For instance, the estimated FeO content in the mantles of the progenitor parent bodies of IID and IVB irons increases from ~7 to ~19 wt % and from ~8 to ~23 wt %, respectively, because of corresponding increases in the core mass fractions by factors of ~2.5 and ~2.6, respectively. These revised values for IID and IVB are comparable to those of IIC (~23 wt %) and SBT (~26 wt %) IMPBs, respectively, with similar Fe/Ni_{CI} ratios in the cores. The reconstructed FeO contents in the progenitor parent bodies of CC IMPBs (12 to 23 wt %) values are well within the range of those of carbonaceous chondrites [17 to 28 wt %; ref. (*63*)] emanating from the CC reservoir. Our findings reveal that with the exception of IIIF, CC IMPBs were consistently more oxidized than their NC counterparts, corroborating the predictions of ref. (*64*).

Sulfur content in the parent cores

Our finding that CC cores with superchondritic HSE/Ni_{CI} ratios only sample the S-poor restite component helps resolve another critical issue related to the chemical composition of the earliest outer Solar System planetesimals—the S content of their parent cores. Fractional crystallization models predict anomalously low S content in CC cores with superchondritic HSE/Ni_{CI} ratios, such as the IID (0 wt % S), IIIF (2 wt % S), and IVB (0 wt % S) cores (Fig. 3C and table S1). This is particularly problematic for the IID irons, which, despite having near-chondritic MVE/Ni_{CI} ratios, appear to sample a nearly S-free core (*7*, *26*). On face value, it means that the primordial materials accreted by the IID IMPB had near-chondritic abundances of all siderophile MVEs except S, which was almost absent. However, there is no evidence of such primordial materials in the CC chondrite record as S abundance always correlates with other MVEs that have comparable condensation temperatures (*65*, *66*). Similar to HSE, Ni, and Co abundances, accounting for the S content in the "missing" component is required to make accurate comparisons between the core composition and the S content in the primordial materials accreted by the progenitor parent body. By factoring in the "missing" component, the parent cores of the progenitor parent bodies of purportedly S-free IID and IVB IMPBs would have contained ~8 and ~9 wt % S, respectively, while those of the other S-poor IIF and IIIF IMPBs would have contained about ~9 and ~4 wt % S, respectively (Fig. 3C and table S1). These values are comparable to the S content in the other CC cores, i.e., IIC (~6 wt % S) and SBT (~8 wt % S), which do not display superchondritic HSE/Ni_{CI} ratios. This suggests that the cores of the earliest CC planetesimals, and consequently, the primordial materials accreted by them, were not as anomalously S-poor as previously believed. The reconstructed S contents of the progenitor CC cores are within the range of three NC cores such as IIIAB, IIIE, and IVA (3 to 9 wt %), although they are still lower than those of the IC and IIAB cores (15 wt % S). Whether S-rich IC and IIAB cores represent a sampling bias in the meteorite record or reflect a fundamental difference in the primordial S contents between NC and CC IMPBs requires further investigation.

Core formation ages of IMPBs

Assuming CC chondrite–like Hf/W ratios in bulk IMPBs, their core formation ages can be determined on the basis of the $\varepsilon^{182}W$ values of iron meteorites from that group (*1*, *2*, *18*). Given that CC irons consistently display higher $\varepsilon^{182}W$ values compared to NC irons, it has been suggested that core formation in the earliest outer Solar System planetesimals generally occurred later than in those from the inner Solar System (fig. S1) (*1*, *18*). Note that the difference between their core formation ages should be smaller if NC IMPBs accreted materials with lower Hf/W ratios, akin to enstatite and ordinary chondrites (*67*, *68*). Our findings suggest that the early-extracted S-rich liquid component in the progenitor parent bodies of IID, IIF, IIIF, and IVB irons is not sampled by iron meteorites from these groups. Thus, the less negative $\varepsilon^{182}W$ values in IID, IIF, IIIF, and IVB irons reflect only the higher $\varepsilon^{182}W$ values of the late-segregated S-poor restite component in the daughter planetesimals and not the bulk $\varepsilon^{182}W$ values of the cores of their progenitor parent bodies. Given that the S-rich component would have undergone core formation before the disruption of the progenitor parent bodies, the timing of the disruption events (likely within ~1 to 2.5 Ma after CAIs; see the earlier discussion) places upper bounds on the unknown $\varepsilon^{182}W$ values of the "missing" component. This implies that core formation in the progenitors of IID, IIF, IIIF, and IVB irons may have begun more than 1 Ma earlier than previously estimated on the basis of iron meteorites alone. This inference is supported by the core formation age of the S-rich SBT IMPB, which is anomalously older than all other CC irons and overlaps with the NC irons having similar S abundance (fig. S1). Therefore, the older core formation age exhibited by SBT irons could be typical of the earliest outer Solar System planetesimals rather than an outlier.

Implications for the dynamics of the early Solar System

Our findings reveal that four of the six CC IMPBs likely formed by accreting the mantle fragments of partially differentiated progenitors that experienced early collisions. The partially differentiated nature of the progenitors of the IID, IIF, IIIF, and IVB IMPBs before the disruption events suggests that these events occurred within a narrow time frame. The need for substantial ^{26}Al to melt the S-poor restite component in the daughter bodies, combined with the core formation age displayed by IID, IIF, IIIF, and IVB irons, indicates that these disruptions likely took place within ~1 to 2.5 Ma after CAIs. Together, our work implies that early planetesimal disruption was prevalent in the CC reservoir.

These predictions, confined to a narrow time frame, have important dynamical implications for the CC reservoir and the evolution of objects during the gas disk phase. For instance, Jupiter's core, and the cores of the other giant planets, may have grown rapidly enough to dynamically excite nearby planetesimals or protoplanets despite the damping effects of the solar nebula (*69*). The impact velocities could have risen enough to cause high-energy impacts or hit-and-run collisions between planetesimals and protoplanets, with the resulting fragments reaccreting into rubble pile daughter bodies (*53*–*55*). This suggests that planetesimal collisions were likely a natural consequence of the growth and migration of protoplanets and the cores of giant planets (*53*, *54*, *70*). While it was previously assumed that the presence of the gas disk would dampen impact velocities, leading to predominantly accretionary collisions (*71*, *72*), our study suggests a different scenario. We argue that disruptive and hit-and-run collisions were not only possible but were also probably common during the gas disk's lifetime. These high-energy events played a crucial role in shaping the early Solar System, driving the fragmentation, reaccretion, and volatile loss that ultimately influenced the composition and evolution of planetary building blocks. This redefines our understanding of planetesimal dynamics during the gas disk phase, highlighting a far more turbulent and complex pathway to planetary formation than previously thought.

To conclude, in this study, we argue that the HSE, Ni, and Co abundance patterns in the IID, IIF, IIIF, and IVB cores can be attributed to their origin from a metal restite component left behind after the extraction of S-rich liquids during early, low-temperature protocore formation in their progenitor parent bodies. These bodies were partially differentiated when they underwent disruptions, and their mantle fragments, including the S-poor metal restite component, reaccreted to form daughter planetesimals. These daughter bodies experienced further core formation with the segregation of the S-poor restite component to form cores, which is eventually sampled by IID, IIF, IIIF, and IVB irons. Therefore, the superchondritic HSE/Ni$_{CI}$ ratios, and their volatility-related fractionation, in CC cores reflect the interplay of protracted core formation and early planetesimal disruptions rather than the accretion of exotic CAI-like materials by their parent bodies.

By accounting for the "missing" S-rich protocore component into the core compositions of CC IMPBs, this work reconciles several apparent discrepancies in the chemical signatures between NC and CC IMPBs, including the S content of the cores, the core mass fractions, and core formation ages. These findings highlight the critical role of early collisions in shaping the chemical evolution of the earliest Solar System planetesimals. If many meteorites in our record sample "second- or later-generation" planetesimals, directly deriving the chemistry of primordial materials accreted by "first-generation" planetesimals, or the protoplanetary disk itself, from these samples may lead to erroneous conclusions.

MATERIALS AND METHODS

Core mass fraction

Previous estimates of core mass fractions for IMPBs are based on the level of HSE enrichment in their cores relative to chondrites (*17*, *19*). This approach relies on two assumptions: (i) HSEs are near-quantitatively segregated into cores during core-mantle differentiation, and (ii) HSE abundances in bulk NC and CC IMPBs resemble those in NC and CC chondrites, respectively. Experimental data at pressures relevant for planetesimal differentiation confirm high metal/silicate partition coefficients for HSEs [$D_i^{metal/silicate} = \sim10^4$ to 10^8; for details, see ref. (*16*) and the references therein], supporting the first assumption. Although there is no direct evidence for the second assumption, near-chondritic element/Ni$_{CI}$ ratios in NC and CC IMPB cores (with exceptions such as IVA and IVB, affected by extreme volatile depletion, and IID, IIF, and IIIF, influenced by additional postdifferentiation processes, as discussed in this study) support its plausibility (*7*, *8*, *16*, *17*). Using the most recent estimates for the abundances of refractory HSEs (Os, Re, Ir, Ru, and Pt) in NC and CC cores (*7*, *8*), we recalculated the core mass fractions of NC and CC IMPBs (table S1). This revision was necessary because refs. (*7*, *8*) used a comprehensive set of both refractory and nonrefractory elements in fractional crystallization models to predict the bulk core compositions of NC and CC IMPBs, whereas refs. (*17*, *19*) relied solely on HSEs in their fractional crystallization models. Given that the HSE abundances in IMPB cores predicted by refs. (*7*, *8*) are generally higher than those of refs. (*17*, *19*) (except for group IC, which is predicted to have lower HSE abundances), the recalculated core-mass fractions in table S1 are generally lower than those predicted by refs. (*7*, *8*).

HSE fractionation in primitive achondrites

The HSE fractionation patterns observed in the IID, IIF, IIIF, and IVB cores are also present in primitive achondrites. For instance, the Pd/Os$_{CI}$ ratios—where Os is more refractory than Pd (*45*)—in ureilites (0.19 to 0.20), brachinites (0.18 to 0.27), acapulcoites (0.18 to 0.27), and lodranites (0.18 to 0.27) are comparable to those found in the IID (0.26) and IVB (0.21) cores and are lower than the IIF (0.48) and IIIF (0.44) cores (*34*–*37*). These ratios are too low to be directly derived from any known chondrite group, as the Pd/Os$_{CI}$ ratios in NC and CC chondrites range from 0.76 to 1.03 (*34*, *36*). When combined with the fractionated Pt/Os$_{CI}$ ratios in primitive achondrites (e.g., 0.74 to 0.84 in ureilites), this suggests that if HSE fractionation was driven by nebular processes, the associated fractionations in Pd/Os$_{CI}$ ratios should be significantly higher because of the larger difference in condensation temperatures between Os and Pd compared to Os and Pt (*34*, *73*). However, this is not observed. Instead, the Pd/Os$_{CI}$ and Pt/Os$_{CI}$ ratios in primitive achondrites are thought to result from silicate-sulfide-metal segregation processes in partially molten planetesimals (*34*–*37*). For instance, the variations in Pd/Os$_{CI}$ and Pt/Os$_{CI}$ ratios in ureilites have been attributed to equilibrium partitioning between S-free solid metal restites and S-rich metallic liquids containing ~25 wt % S, followed by their segregation (*34*). Pd and Pt have lower solid/liquid metal partition coefficients compared to Os (fig. S2) (*46*), and their fractionation based on the S content has been used to constrain the S

content in the metallic liquid that segregated from the S-free solid metal restite (*34*).

Elemental partitioning between the S-free solid and the S-bearing liquid metal

Elemental partitioning between the S-free solid metal restite and the S-bearing liquid metal was calculated using mass balance equations in batch melting models. The mass balance of any siderophile/chalcophile element i between the bulk metal $\left(M_i^{\mathrm{B}}\right)$, solid metal (M_i^{S}), and the liquid metal (M_i^{L}) can be written as

$$M_i^{\mathrm{B}} = M_i^{\mathrm{S}} + M_i^{\mathrm{L}} \tag{1}$$

Relating the mass of an element to the mass of the reservoir (m) and concentration (C_i) of the element in that reservoir we get

$$m_{\mathrm{B}} C_i^{\mathrm{B}} = m_{\mathrm{S}} C_i^{\mathrm{S}} + m_{\mathrm{L}} C_i^{\mathrm{L}} \tag{2}$$

The m_{B} term can be expanded to yield

$$\left(m_{\mathrm{S}} + m_{\mathrm{L}}\right) C_i^{\mathrm{B}} = m_{\mathrm{S}} C_i^{\mathrm{S}} + m_{\mathrm{L}} C_i^{\mathrm{L}} \tag{3}$$

Dividing by m_{L} terms on both sides yields

$$\left(m_{\mathrm{S}}/m_{\mathrm{L}} + 1\right) C_i^{\mathrm{B}} = \left(m_{\mathrm{S}}/m_{\mathrm{L}}\right) \cdot C_i^{\mathrm{S}} + C_i^{\mathrm{L}} \tag{4}$$

C_i^{S} and C_i^{L} are related by the partition coefficient between the two phases

$$D_i^{\mathrm{S/L}} = C_i^{\mathrm{S}} / C_i^{\mathrm{L}} \tag{5}$$

Equations 4 and 5 can be combined to yield the following equation

$$C_i^{\mathrm{S}} / C_i^{\mathrm{B}} = \left[\left(m_{\mathrm{S}}/m_{\mathrm{L}} + 1\right)\right] / \left[m_{\mathrm{S}}/m_{\mathrm{L}} + \left(1/D_i^{\mathrm{S/L}}\right)\right] \tag{6}$$

To calculate the $C_i^{\mathrm{S}}/C_{\mathrm{Ni}}^{\mathrm{S}}$ ratio, Eq. 6 can be rewritten by dividing all terms in Eq. 6 by the corresponding terms for Ni

$$\begin{aligned}&\left[C_i^{\mathrm{S}}/C_i^{\mathrm{B}}\right] / \left[C_{\mathrm{Ni}}^{\mathrm{S}}/C_{\mathrm{Ni}}^{\mathrm{B}}\right] \\ &= \left[m_{\mathrm{S}}/m_{\mathrm{L}} + \left(1/D_{\mathrm{Ni}}^{\mathrm{S/L}}\right)\right] / \left[m_{\mathrm{S}}/m_{\mathrm{L}} + \left(1/D_i^{\mathrm{S/L}}\right)\right]\end{aligned} \tag{7}$$

Here, C_i^{B}, the concentration of an element in the bulk metal of an IMPB, is equivalent to its concentration in the parent core if the entire metal had segregated into the core. This value corresponds to the concentration of the element in the IMPB divided by its core-to-mantle mass ratio. Assuming CI chondrite–like elemental concentrations in the bulk IMPB, and considering the cancellation of the core-to-mantle mass ratio terms because of the division of C_i^{B} by $C_{\mathrm{Ni}}^{\mathrm{B}}$ on the left-hand side of Eq. 7, the equation simplifies to

$$\begin{aligned}&\left[C_i^{\mathrm{S}}/C_i^{\mathrm{CI}}\right] / \left[C_{\mathrm{Ni}}^{\mathrm{S}}/C_{\mathrm{Ni}}^{\mathrm{CI}}\right] \\ &= \left[m_{\mathrm{S}}/m_{\mathrm{L}} + \left(1/D_{\mathrm{Ni}}^{\mathrm{S/L}}\right)\right] / \left[m_{\mathrm{S}}/m_{\mathrm{L}} + \left(1/D_i^{\mathrm{S/L}}\right)\right]\end{aligned} \tag{8}$$

The left-hand side of Eq. 8 can now simply be rewritten as

$$\left(C_t^{\mathrm{S}}/C_{\mathrm{Ni}}^{\mathrm{S}}\right)_{\mathrm{CI}} = \left[m_{\mathrm{S}}/m_{\mathrm{L}} + \left(1/D_{\mathrm{Ni}}^{\mathrm{S/L}}\right)\right] / \left[m_{\mathrm{S}}/m_{\mathrm{L}} + \left(1/D_i^{\mathrm{S/L}}\right)\right] \tag{9}$$

Equation 9 has two unknowns—$m_{\mathrm{S}}/m_{\mathrm{L}}$ and $D_i^{\mathrm{S/L}}$ (partition coefficient of an element between the solid and the liquid metal). C_i^{S} values for ureilites are compiled from ref. (*37*)—the most comprehensive compilation for siderophile and chalcophile elements in ureilites—whereas for the C_i^{S} values of IID, IIF, IIIF, and IVB IMPBs, the core compositions predicted by refs. (*7*, *48*) are used. Given that the partitioning of an element between the S-free solid metal restite and the S-rich liquid metal is primarily controlled by the latter, parameterized $D_i^{\mathrm{S/L}}$ equations from ref. (*46*) as a function of S content in the liquid metal are used. The $D_i^{\mathrm{S/L}}$ parametrized equations are written in the form of

$$\ln D_i^{\mathrm{S/L}} = \ln D_{i,0} + \beta \ln(\mathrm{Fe-domains}) \tag{10}$$

The values of fixed terms $D_{\mathrm{i,0}}$ and β are reported in ref. (*46*) and tabulated in table S3. The Fe-domains term can be written as

$$\mathrm{Fe-domains} = \left(1 - 2X_{\mathrm{S}}\right) / \left(1 - X_{\mathrm{S}}\right) \tag{11}$$

where X_{S} is the mole fraction of the S content in the liquid.

We used a Bayesian MCMC approach using the probabilistic programming library PyMC to determine the S content in the liquid metal and the mass ratio of solid to liquid metal $(m_{\mathrm{S}}/m_{\mathrm{L}})$ (Fig. 1 and table S2). This approach was designed to best replicate the observed abundances of HSEs, Ni, and Co in the restite component. We assigned uniform prior distributions to both model parameters: 0 to 100 wt % for the S content and 0 to 1000 for $m_{\mathrm{S}}/m_{\mathrm{L}}$. The HSE concentrations of IMPBs, normalized to CI and Ni, were assumed to carry a 5% Gaussian uncertainty. We sampled the posterior distributions using the No-U-Turn Sampler implemented in PyMC. To ensure sampling efficiency and convergence, we performed 1000 tuning steps followed by 2000 posterior draws, with a target acceptance probability of 0.95. From the resulting posterior distributions, we report the mean and standard deviation for both parameters.

Thermal evolution of planetesimals reaccreted from collisional fragments

We model the thermal evolution of planetesimals reaccreted from collisional fragments by considering heat from the short-lived radioisotope ^{26}Al (fig. S3). We assume that the reaccreted planetesimals are sufficiently large [e.g., ~100 km in radius, as inferred from the cooling rates of IIAB, IVA, and IVB iron meteorites (*74*–*76*)] such that conductive cooling can be neglected for its interior temperature evolution in over a million-year timescale [e.g., (*77*)]. We also neglect the effect of latent heat, whose effect can be expected to be relatively small. In this case, the interior temperature of a reaccreted planetesimal is controlled by heating from ^{26}Al such that it varies with time following

$$\Delta T = \lambda^{-1} \left(Q_0/C_{\mathrm{p}}\right) \left(e^{-\lambda t_0} - e^{-\lambda t}\right) \tag{12}$$

where ΔT is the temperature increase after reaccretion, $Q_0 = 1.5 \times 10^{-7}$ W/kg is the heat of heat production from ^{26}Al decay at the time of CAI (*78*), $C_{\mathrm{p}} = 1000$ J/(kg·K) is the specific heat capacity, $\lambda = 3 \times 10^{-14}$ s^{-1} is the decay constant of ^{26}Al, t is the time after CAI, and t_0 is the time (after CAI) of parent planetesimal disruption and daughter planetesimal reaccretion.

While the reaccretion timescales are likely short [e.g., ~1 year or less; (*79*)], the sizes of the collisional fragments involved in reassembly can vary widely. Observational constraints, such as the cooling histories of ordinary chondrite parent bodies, have been interpreted as evidence for rapid heat loss during the fragmentation-reassembly process [e.g., ref. (*80*)]. Motivated by such findings, ref. (*81*) modeled the thermal evolution of materials in rubble pile formation and

suggested that catastrophic fragmentation can lead to significant heat loss, even over short reassembly timescales (e.g., ≤1 year), because of the generation of numerous small fragments. To account for this possibility, we explore different degrees of initial cooling before reassembly and examine the implications of these variations using a range of plausible end-member scenarios (fig. S3).

Supplementary Materials

This PDF file includes:

Figs. S1 to S3
Tables S1 to S3
References

REFERENCES AND NOTES

1. T. S. Kruijer, C. Burkhardt, G. Budde, T. Kleine, Age of Jupiter inferred from the distinct genetics and formation times of meteorites. *Proc. Natl. Acad. Sci. U.S.A.* **114**, 6712–6716 (2017).
2. T. S. Kruijer, M. Touboul, M. Fischer-Godde, K. R. Bermingham, R. J. Walker, T. Kleine, Protracted core formation and rapid accretion of protoplanets. *Science* **344**, 1150–1154 (2014).
3. J. I. Goldstein, E. R. D. Scott, N. L. Chabot, Iron meteorites: Crystallization, thermal history, parent bodies, and origin. *Chem. Erde* **69**, 293–325 (2009).
4. E. R. D. Scott, J. T. Wasson, Classification and properties of iron meteorites. *Rev. Geophys.* **13**, 527–546 (1975).
5. N. L. Chabot, H. Haack, "Evolution of asteroidal cores evolution of asteroidal cores," in *Meteorites and the Early Solar System II*, D. S. Lauretta, H. Y. McSween, Eds. (University of Arizona Press, 2006), pp. 747–771.
6. E. R. D. Scott, Chemical fractionation in iron meteorites and its interpretation. *Geochim. Cosmochim. Acta* **36**, 1205–1236 (1972).
7. B. Zhang, N. L. Chabot, A. E. Rubin, Compositions of carbonaceous-type asteroidal cores in the early solar system. *Sci. Adv.* **8**, eabo5781 (2022).
8. B. Zhang, N. L. Chabot, N. L. Chabot, Compositions of iron-meteorite parent bodies: Constraints on the structure of the protoplanetary disk. *Proc. Natl. Acad. Sci. U.S.A.* **121**, e2306995121 (2024).
9. D. S. Grewal, P. D. Asimow, Origin of the superchondritic carbon/nitrogen ratio of the bulk silicate Earth – An outlook from iron meteorites. *Geochim. Cosmochim. Acta* **344**, 146–159 (2023).
10. D. S. Grewal, R. Dasgupta, B. Marty, A very early origin of isotopically distinct nitrogen in inner Solar System protoplanets. *Nat. Astron.* **5**, 356–364 (2021).
11. M. M. Hirschmann, E. A. Bergin, G. A. Blake, F. J. Ciesla, J. Li, Early volatile depletion on planetesimals inferred from C–S systematics of iron meteorite parent bodies. *Proc. Natl. Acad. Sci. U.S.A.* **118**, e2026779118 (2021).
12. D. S. Grewal, J. D. Seales, R. Dasgupta, Internal or external magma oceans in the earliest protoplanets – Perspectives from nitrogen and carbon fractionation. *Earth Planet. Sci. Lett.* **598**, 117847 (2022).
13. D. S. Grewal, Origin of nitrogen isotopic variations in the rocky bodies of the solar system. *Astrophys. J.* **937**, 123 (2022).
14. D. S. Grewal, T. Sun, S. Aithala, T. Hough, R. Dasgupta, L. Y. Yeung, E. A. Schauble, Limited nitrogen isotopic fractionation during core-mantle differentiation in rocky protoplanets and planets. *Geochim. Cosmochim. Acta* **338**, 347–364 (2022).
15. D. S. Grewal, N. X. Nie, B. Zhang, A. Izidoro, P. D. Asimow, Accretion of the earliest inner Solar System planetesimals beyond the water snowline. *Nat. Astron.* **8**, 290–297 (2024).
16. D. S. Grewal, S. Bhattacharjee, B. Zhang, N. X. Nie, Y. Miyazaki, Enrichment of moderately volatile elements in first-generation planetesimals of the inner Solar System. *Sci. Adv.* **11**, eadq7848 (2025).
17. C. D. Hilton, R. D. Ash, R. J. Walker, Chemical characteristics of iron meteorite parent bodies. *Geochim. Cosmochim. Acta* **318**, 112–125 (2022).
18. F. Spitzer, C. Burkhardt, F. Nimmo, T. Kleine, Nucleosynthetic Pt isotope anomalies and the Hf-W chronology of core formation in inner and outer solar system planetesimals. *Earth Planet. Sci. Lett.* **576**, 117211 (2021).
19. E. M. Chiappe, R. D. Ash, R. J. Walker, Age, genetics, and crystallization sequence of the group IIIE iron meteorites. *Geochim. Cosmochim. Acta* **354**, 51–61 (2023).
20. H. A. Tornabene, R. D. Ash, R. J. Walker, K. R. Bermingham, Genetics, age, and crystallization history of group IC iron meteorites. *Geochim. Cosmochim. Acta* **340**, 108–119 (2023).
21. D. S. Grewal, S. Bhattacharjee, G.-D. Mardaru, P. D. Asimow, Tracing the origin of volatiles on Earth using nitrogen isotope ratios in iron meteorites. *Geochim. Cosmochim. Acta* **388**, 34–47 (2025).
22. A. Morbidelli, K. Baillié, K. Batygin, S. Charnoz, T. Guillot, D. C. Rubie, T. Kleine, Contemporary formation of early Solar System planetesimals at two distinct radial locations. *Nat. Astron.* **6**, 72–79 (2021).
23. A. E. Rubin, Carbonaceous and noncarbonaceous iron meteorites: Differences in chemical, physical, and collective properties. *Meteorit. Planet. Sci.* **53**, 2357–2371 (2018).
24. N. L. Chabot, Sulfur contents of the parental metallic cores of magmatic iron meteorites. *Geochim. Cosmochim. Acta* **68**, 3607–3618 (2004).
25. J. T. Wasson, Trapped melt in IIIAB irons; solid/liquid elemental partitioning during the fractionation of the IIIAB magma. *Geochim. Cosmochim. Acta* **63**, 2875–2889 (1999).
26. J. T. Wasson, H. Huber, Compositional trends among IID irons; their possible formation from the P-rich lower magma in a two-layer core. *Geochim. Cosmochim. Acta* **70**, 6153–6167 (2006).
27. C. M. O. Alexander, Quantitative models for the elemental and isotopic fractionations in chondrites: The carbonaceous chondrites. *Geochim. Cosmochim. Acta* **254**, 277–309 (2019).
28. A. J. Campbell, M. Humayun, Compositions of group IVB iron meteorites and their parent melt. *Geochim. Cosmochim. Acta* **69**, 4733–4744 (2005).
29. H. Terasaki, D. J. Frost, D. C. Rubie, F. Langenhorst, Percolative core formation in planetesimals. *Earth Planet. Sci. Lett.* **273**, 132–137 (2008).
30. A. Néri, J. Guignard, M. Monnereau, M. J. Toplis, G. Quitté, Metal segregation in planetesimals: Constraints from experimentally determined interfacial energies. *Earth Planet. Sci. Lett.* **518**, 40–52 (2019).
31. T. Yoshino, M. J. Walter, T. Katsura, Core formation in planetesimals triggered by permeable flow. *Nature* **422**, 154–157 (2003).
32. G. D. Bromiley, The geochemical legacy of low-temperature, percolation-driven core formation in planetesimals. *Earth Moon Planets* **127**, 4 (2023).
33. A. Holzheid, M. D. Schmitz, T. L. Grove, Textural equilibria of iron sulfide liquids in partly molten silicate aggregates and their relevance to core formation scenarios. *J. Geophys. Res. Solid Earth* **105**, 13555–13567 (2000).
34. K. Rankenburg, M. Humayun, A. D. Brandon, J. S. Herrin, Highly siderophile elements in ureilites. *Geochim. Cosmochim. Acta* **72**, 4642–4659 (2008).
35. Y. Hidaka, N. Shirai, A. Yamaguchi, M. Ebihara, Siderophile element characteristics of acapulcoite–lodranites and winonaites: Implications for the early differentiation processes of their parent bodies. *Meteorit. Planet. Sci.* **54**, 1153–1166 (2019).
36. J. M. D. Day, R. J. Walker, R. D. Ash, Y. Liu, D. Rumble, A. J. Irving, C. A. Goodrich, K. Tait, W. F. McDonough, L. A. Taylor, Origin of felsic achondrites Graves Nunataks 06128 and 06129, and ultramafic brachinites and brachinite-like achondrites by partial melting of volatile-rich primitive parent bodies. *Geochim. Cosmochim. Acta* **81**, 94–128 (2012).
37. P. H. Warren, F. Ulff-Møller, H. Huber, G. W. Kallemeyn, Siderophile geochemistry of ureilites: A record of early stages of planetesimal core formation. *Geochim. Cosmochim. Acta* **70**, 2104–2126 (2006).
38. J. M. Sunshine, H. C. Connolly, T. J. McCoy, S. J. Bus, L. M. La Croix, Ancient asteroids enriched in refractory inclusions. *Science* **320**, 514–517 (2008).
39. G. A. Brennecka, C. Burkhardt, G. Budde, T. S. Kruijer, F. Nimmo, T. Kleine, Astronomical context of Solar System formation from molybdenum isotopes in meteorite inclusions. *Science* **370**, 837–840 (2020).
40. G. Budde, C. Burkhardt, T. Kleine, Molybdenum isotopic evidence for the late accretion of outer Solar System material to Earth. *Nat. Astron.* **3**, 736–741 (2019).
41. J. F. J. Bryson, G. A. Brennecka, Constraints on chondrule generation, disk dynamics, and asteroid accretion from the compositions of carbonaceous meteorites. *Astrophys. J.* **912**, 163 (2021).
42. K. R. Bermingham, H. A. Tornabene, R. J. Walker, L. V. Godfrey, B. S. Meyer, P. Piccoli, S. J. Mojzsis, The non-carbonaceous nature of Earth's late-stage accretion. *Geochim. Cosmochim. Acta* **392**, 38–51 (2025).
43. C. A. Goodrich, J. H. Jones, J. L. Berkley, Origin and evolution of the ureilite parent magmas: Multi-stage igneous activity on a large parent body. *Geochim. Cosmochim. Acta* **51**, 2255–2273 (1987).
44. K. Keil, T. J. McCoy, Acapulcoite-lodranite meteorites: Ultramafic asteroidal partial melt residues. *Geochemistry* **78**, 153–203 (2018).
45. B. J. Wood, D. J. Smythe, T. Harrison, The condensation temperatures of the elements: A reappraisal. *Am. Mineral.* **104**, 844–856 (2019).
46. N. L. Chabot, E. A. Wollack, W. F. McDonough, R. D. Ash, S. A. Saslow, Experimental determination of partitioning in the Fe-Ni system for applications to modeling meteoritic metals. *Meteorit. Planet. Sci.* **52**, 1133–1145 (2017).
47. R. Brett, P. M. Bell, Melting relations in the Fe-rich portion of the system FeFeS at 30 kb pressure. *Earth Planet. Sci. Lett.* **6**, 479–482 (1969).
48. B. Zhang, N. L. Chabot, A. E. Rubin, M. Humayun, J. S. Boesenberg, D. van Niekerk, Chemical study of group IIIF iron meteorites and the potentially related pallasites Zinder and Northwest Africa 1911. *Geochim. Cosmochim. Acta* **323**, 202–219 (2022).
49. M. Weyrauch, J. Zipfel, S. Weyer, The relationship of CH, CB, and CR chondrites: Constraints from trace elements and Fe-Ni isotope systematics in metal. *Geochim. Cosmochim. Acta* **308**, 291–309 (2021).

50. B. Zhang, N. L. Chabot, A. E. Rubin, Compositions of iron-meteorite parent bodies constrain the structure of the protoplanetary disk. *Proc. Natl. Acad. Sci. U.S.A.* **121**, e2306995121 (2024).
51. S. T. Stewart, Z. M. Leinhardt, Collisions between gravity-dominated bodies. II. The diversity of impact outcomes during the end stage of planet formation. *Astrophys. J.* **751**, 32 (2012).
52. E. Asphaug, Similar-sized collisions and the diversity of planets. *Geochemistry* **70**, 199–219 (2010).
53. C. Agnor, E. Asphaug, Accretion efficiency during planetary collisions. *Astrophys. J.* **613**, L157–L160 (2004).
54. E. Asphaug, C. B. Agnor, Q. Williams, Hit-and-run planetary collisions. *Nature* **439**, 155–160 (2006).
55. E. R. D. Scott, K. Keil, J. I. Goldstein, E. Asphaug, W. F. Bottke, N. A. Moskovitz, "Early impact history and dynamical origin of differentiated meteorites and asteroids," in *Asteroids IV* (University of Arizona Press, 2015), pp. 573–595.
56. C. A. Goodrich, W. K. Hartmann, D. P. O'Brien, S. J. Weidenschilling, L. Wilson, P. Michel, M. Jutzi, Origin and history of ureilitic material in the solar system: The view from asteroid 2008 TC3 and the Almahata Sitta meteorite. *Meteorit. Planet. Sci.* **50**, 782–809 (2015).
57. N. Rai, H. Downes, C. Smith, Ureilite meteorites provide a new model of early planetesimal formation and destruction. *Geochem. Perspect. Lett.* **14**, 20–25 (2020).
58. H. Downes, D. W. Mittlefehldt, N. T. Kita, J. W. Valley, Evidence from polymict ureilite meteorites for a disrupted and re-accreted single ureilite parent asteroid gardened by several distinct impactors. *Geochim. Cosmochim. Acta* **72**, 4825–4844 (2008).
59. J. S. Herrin, M. E. Zolensky, M. Ito, L. Le, D. W. Mittlefehldt, P. Jenniskens, A. J. Ross, M. H. Shaddad, Thermal and fragmentation history of ureilitic asteroids: Insights from the Almahata Sitta fall. *Meteorit. Planet. Sci.* **45**, 1789–1803 (2010).
60. C. A. Goodrich, E. R. D. Scott, A. M. Fioretti, Ureilitic breccias: Clues to the petrologic structure and impact disruption of the ureilite parent asteroid. *Chemie der Erde* **64**, 283–327 (2004).
61. P. H. Warren, Stable-isotopic anomalies and the accretionary assemblage of the Earth and Mars: A subordinate role for carbonaceous chondrites. *Earth Planet. Sci. Lett.* **311**, 93–100 (2011).
62. A. S. Buono, D. Walker, The Fe-rich liquidus in the Fe-FeS system from 1bar to 10GPa. *Geochim. Cosmochim. Acta* **75**, 2072–2087 (2011).
63. E. Jarosewich, Chemical analyses of meteorites at the Smithsonian Institution: An update. *Meteorit. Planet. Sci.* **41**, 1381–1382 (2006).
64. Z. Zhang, Ice sublimation in planetesimals formed at the outward migrating snowline. *Astrophys. J. Lett.* **956**, L25 (2023).
65. N. Braukmüller, F. Wombacher, D. C. Hezel, R. Escoube, C. Münker, The chemical composition of carbonaceous chondrites: Implications for volatile element depletion, complementarity and alteration. *Geochim. Cosmochim. Acta* **239**, 17–48 (2018).
66. C. M. O. D. Alexander, J. G. Wynn, R. Bowden, Sulfur abundances and isotopic compositions in bulk carbonaceous chondrites and insoluble organic material: Clues to elemental and isotopic fractionations of volatile chalcophiles. *Meteorit. Planet. Sci.* **57**, 334–351 (2022).
67. J. L. Hellmann, J. A. Van Orman, T. Kleine, Hf-W isotope systematics of enstatite chondrites: Parent body chronology and origin of Hf-W fractionations among chondritic meteorites. *Earth Planet. Sci. Lett.* **626**, 118518 (2024).
68. J. L. Hellmann, G. Budde, L. N. Willhite, R. J. Walker, Hf–W isotope systematics of bulk chondrites: Implications for early Solar System evolution. *Geochim. Cosmochim. Acta* **387**, 38–52 (2024).
69. S. N. Raymond, A. Izidoro, Origin of water in the inner Solar System: Planetesimals scattered inward during Jupiter and Saturn's rapid gas accretion. *Icarus* **297**, 134–148 (2017).
70. P. J. Carter, S. T. Stewart, Colliding in the shadows of giants: Planetesimal collisions during the growth and migration of gas giants. *Planet. Sci. J.* **1**, 45 (2020).
71. K. J. Walsh, H. F. Levison, Planetesimals to terrestrial planets: Collisional evolution amidst a dissipating gas disk. *Icarus* **329**, 88–100 (2019).
72. A. Morbidelli, J. I. Lunine, D. P. O'Brien, S. N. Raymond, K. J. Walsh, Building terrestrial planets. *Annu. Rev. Earth Planet. Sci.* **40**, 251–275 (2012).
73. A. J. Campbell, S. B. Simon, M. Humayun, L. Grossman, Chemical evolution of metal in refractory inclusions in CV3 chondrites. *Geochim. Cosmochim. Acta* **67**, 3119–3134 (2003).
74. J. Yang, J. I. Goldstein, J. R. Michael, P. G. Kotula, E. R. D. Scott, Thermal history and origin of the IVB iron meteorites and their parent body. *Geochim. Cosmochim. Acta* **74**, 4493–4506 (2010).
75. J. Yang, J. I. Goldstein, Metallographic cooling rates of the IIIAB iron meteorites. *Geochim. Cosmochim. Acta* **70**, 3197–3215 (2006).
76. J. Yang, J. I. Goldstein, E. R. D. Scott, Metallographic cooling rates and origin of IVA iron meteorites. *Geochim. Cosmochim. Acta* **72**, 3043–3061 (2008).
77. R. E. Grimm, H. Y. McSween, Heliocentric zoning of the asteroid belt by aluminum-26 heating. *Science* **259**, 653–655 (1993).
78. O. Šrámek, L. Milelli, Y. Ricard, S. Labrosse, Thermal evolution and differentiation of planetesimals and planetary embryos. *Icarus* **217**, 339–354 (2012).
79. S. G. Love, T. J. Ahrens, Catastrophic impacts on gravity dominated asteroids. *Icarus* **124**, 141–155 (1996).
80. M. P. Lucas, N. Dygert, J. Ren, M. A. Hesse, N. R. Miller, H. Y. McSween, Evidence for early fragmentation-reassembly of ordinary chondrite (H, L, and LL) parent bodies from REE-in-two-pyroxene thermometry. *Geochim. Cosmochim. Acta* **290**, 366–390 (2020).
81. J. Ren, M. A. Hesse, N. Dygert, M. P. Lucas, Deterministic model for asteroid thermal evolution with fragmentation and reassembly into a gravitational aggregate. *J. Geophys. Res. Planets* **129**, e2023JE007898 (2024).
82. N. L. Chabot, B. Zhang, A revised trapped melt model for iron meteorites applied to the IIIAB group. *Meteorit. Planet. Sci.* **57**, 200–227 (2022).

Acknowledgments: We thank A. P. Vyas for helping to improve the clarity of our communication. **Funding:** This study was supported by startup funds from Yale and ASU to D.S.G. T.S.K was supported by Laboratory Directed Research and Development Program at Lawrence Livermore National Laboratory (grant 23-ERD-003). **Author contributions:** Conceptualization: D.S.G. and Z.Z. Methodology: D.S.G. and Z.Z. Validation: D.S.G., Z.Z., and V.M. Formal analysis: D.S.G., Z.Z., and V.M. Data curation: D.S.G. and V.M. Software: V.M. Resources: D.S.G. Investigation: D.S.G. Visualization: D.S.G. and Z.Z. Funding acquisition: D.S.G. Project administration: D.S.G. Supervision: D.S.G. Writing—original draft: D.S.G. Writing—review and editing: D.S.G., Z.Z., T.S.K., W.F.B., and S.T.S. **Competing interests:** The authors declare that they have no competing interests. **Data and materials availability:** All data needed to evaluate the conclusions in the paper are present in the paper and/or the Supplementary Materials.

Submitted 27 January 2025
Accepted 29 August 2025
Published 1 October 2025
10.1126/sciadv.adw1668